Charge conversion enables quantification of the proximity between a normally-neutral μ-conotoxin (GIIIA) site and the Na^+ channel pore

Ronald A. Li[a], Kazuki Sato[b], Kyoko Kodama[b], Toshiyuki Kohno[c], Tian Xue[a], Gordon F. Tomaselli[a], Eduardo Marbán[a,*]

[a] *Institute of Molecular Cardiobiology, The Johns Hopkins University School of Medicine, 720 Rutland Avenue/Ross 844, Baltimore, MD 21205, USA*
[b] *Fukuoka Womens University, Fukuoka 813-8529, Japan*
[c] *Mitsubishi Kagaku Institute of Life Sciences, Machida, Tokyo 194-8511, Japan*

Received 29 October 2001; revised 12 December 2001; accepted 13 December 2001

First published online 8 January 2002

Edited by Maurice Montal

Abstract **μ-Conotoxin (μ-CTX) inhibits Na^+ flux by obstructing the Na^+ channel pore. Previous studies of μ-CTX have focused only on charged toxin residues, ignoring the neutral sites. Here we investigated the proximity between the C-terminal neutral alanine (A22) of μ-CTX and the Na^+ channel pore by replacing it with the negatively charged glutamate. The analog A22E and wild-type (WT) μ-CTX exhibited identical nuclear magnetic resonance spectra except at the site of replacement, verifying that they have identical backbone structures. A22E significantly reduced μ-CTX affinity for WT μ1 Na^+ channels (90-fold ↓), as if the inserted glutamate repels the anionic pore receptor. We then looked for the interacting partner(s) of residue 22 by determining the potency of block of Y401K, Y401A, E758Q, D762K, D762A, E765K, E765A and D1241K channels by WT μ-CTX and A22E, followed by mutant cycle analysis to assess their individual couplings. Our results show that A22E interacts strongly with E765K from domain II (DII) ($\Delta\Delta G = 2.2 \pm 0.1$ vs. < 1 kcal/mol for others). We conclude that μ-CTX residue 22 closely associates with the DII pore in the toxin-bound channel complex. The approach taken may be further exploited to study the proximity of other neutral toxin residues with the Na^+ channel pore.** © **2002 Federation of European Biochemical Societies. Published by Elsevier Science B.V. All rights reserved.**

Key words: Sodium channel; μ-Conotoxin; Protein engineering; Mutagenesis; Mutant cycle analysis

1. Introduction

μ-Conotoxin (μ-CTX) GIIIA is a 22-residue pore-blocking peptide isolated from the sea snail *Conus geographus* [1,2]. μ-CTX is known to contain three intra-molecular disulfide bonds that impart to the toxin backbone extreme structural rigidity [3]. In fact, this rigidity and the well-defined three-dimensional (3D) structure of μ-CTX [4–7] have made it an excellent probe for studying the much less certain Na^+ channel pore structure. While chemically distinct from the puffer-fish-derived tetrodotoxin (TTX) and the red-tide saxitoxin (STX), μ-CTX shows similar biological actions. Belonging to the same class as TTX and STX (i.e. site I blockers [8]), μ-CTX exerts its toxicity by binding to the pore of voltage-gated Na^+ channels [2,9–12]. The TTX/STX and μ-CTX sites overlap but are not identical [9,12,13]. Indeed, the large physical size of μ-CTX (molecular weight = ∼2600 vs. ∼300 for TTX/STX) distinguishes its receptor from the more compact TTX/STX site [12,14–17].

High-affinity μ-CTX binding results from the summed effects of numerous weaker toxin–channel interactions [5,6,11,12,15–17,22]. Although extensive efforts have been made to identify these interactions [16–18], previous studies have focused only on charged, mostly cationic, μ-CTX residues while leaving the neutral sites unexplored. In this study, we investigated the molecular interactions between the neutral alanine at the C-terminal end of μ-CTX (i.e. A22) and the Na^+ channel pore. We reasoned that replacing A22 with a charged amino acid should create attractive or repulsive forces of interactions depending on the complementarity of the inserted charge and the nearby pore residues in the toxin-bound channel complex. Using this strategy, we found that μ-CTX residue 22 is closely associated with the domain II (DII) pore region in the toxin-bound channel complex.

2. Materials and methods

2.1. Peptide synthesis, purification and structural analysis

μ-CTX (GIIIA) analogs were synthesized by the solid-phase method with 9-fluorenylmethoxycarbonyl chemistry and purified by successive chromatography with gel filtration, ion exchange, and reversed-phase high-performance liquid chromatography as previously described [5]. Disulfide bonds were formed by air oxidation. Peptide composition was verified by quantitative amino acid analysis and/or mass spectroscopy. 3D structural differences of peptides were studied by ^1H nuclear magnetic resonance (NMR) spectroscopy using a Bruker Avance-500 spectrometer (Bruker, Ibaragi, Japan) operating at 500 MHz for proton frequency. 3D molecular models of peptides were created in Insight/Discover (Molecular Simulations, San Diego, CA, USA). The steepest descents and conjugate gradients algorithms were used for energy minimization. The coordinates for μ-CTX were obtained from the Brookhaven Protein Data Bank (1TCG [6]).

2.2. Site-directed mutagenesis and heterologous expression

The gene encoding the wild-type (WT) rat skeletal muscle (μ1) sodium channel α-subunit was cloned into the pGFP-IRES vector. Mutations were created using polymerase chain reaction with overlapping mutagenic primers, and confirmed by DNA sequencing. Channel constructs were expressed in tsA-201 cells using Lipofectamine Plus transfection kit (Gibco-BRL, Gaithersburg, MD, USA) according to the manufacturer's protocol. Transfected cells were incubated at 37°C in a humidified atmosphere of 95% O_2–5% CO_2 for 48–72 h for channel expression before electrical recordings.

*Corresponding author. Fax: (1)-410-955 7953.
E-mail address: marban@jhmi.edu (E. Marbán).

PII: S0014-5793(01)03316-6

2.3. Electrophysiology

Electrophysiological recordings were performed at room temperature using whole-cell patch clamp. Transfected cells were identified visually by the green epifluorescence of expressed green fluorescent protein during illumination at 488 ± 10 nM. Pipette electrodes had final tip resistances of 1–3 MΩ. All recordings were performed at room temperature in a bath solution containing (in mM): 140 NaCl, 5 KCl, 2 $CaCl_2$, 1 $MgCl_2$, 10 HEPES, 10 glucose, pH adjusted to 7.4 with NaOH. Designated amounts of μ-CTX GIIIA or its derivatives were added to the bath when required and superfused continuously during the experiment. The internal solution for patch recordings contained (in mM): 35 NaCl, 105 CsF, 1 $MgCl_2$, 10 HEPES, 1 EGTA, pH adjusted to 7.2 with CsOH.

2.4. Data analysis

Half-blocking concentrations (IC_{50}) for μ-CTX were determined by fitting the dose–response data to the following binding isotherm:

$$I/I_0 = 1/\{1 + ([\text{toxin}]/IC_{50})\}$$

where [toxin] is the toxin concentration, I_0 and I are the peak currents measured from a step depolarization to −10 mV for 50 ms from a holding potential of −100 mV before and after the application of the blocker, respectively.

For kinetic analysis of μ-CTX block, the time course of the change of peak sodium currents elicited by depolarization to −10 mV from a holding potential of −100 mV during toxin washin or washout was fitted to a single-exponential function using a non-linear least-squares method for estimation of the time constants τ_{on} and τ_{off}. The pseudo-first-order association rate constant (k_{on}) and the first-order dissociation rate constant (k_{off}) were calculated from these time constants using the following relations:

$$k_{off} = 1/\tau_{off}$$

$$k_{on} = ((1/\tau_{on}) - (1/\tau_{off}))/[\mu - \text{CTX}]$$

For mutant cycle analysis, coupling coefficients (Ω) and interaction energies ($\Delta\Delta G$) for various mutant toxin–channel pairs were calculated from the corresponding IC_{50} values using the following equation:

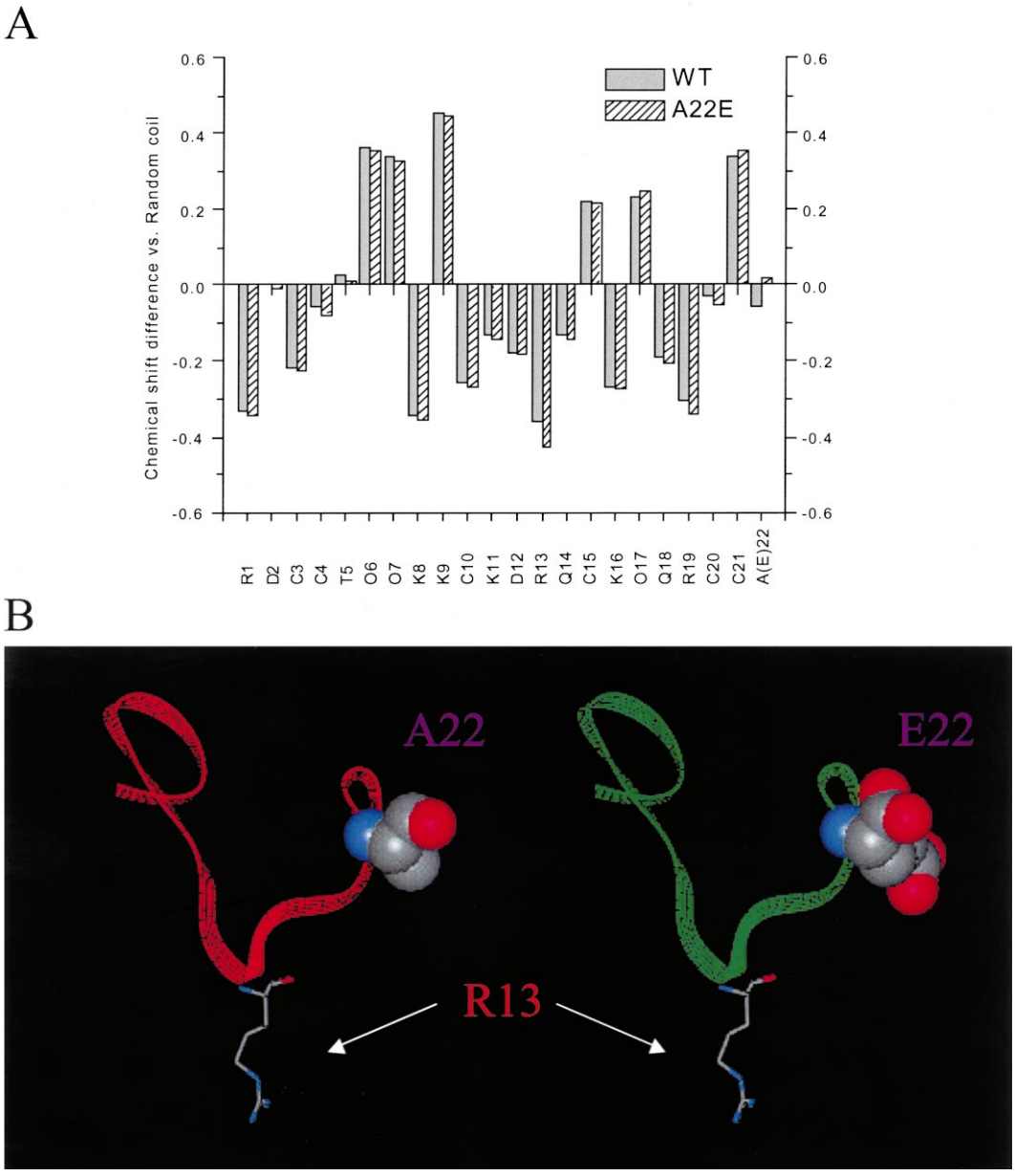

Fig. 1. 3D structures of μ-CTX and A22E. A: NMR chemical shift difference between the α-protons of μ-CTX (solid) and A22E (hatched) residues and the random coil values. B: 3D model structures of WT μ-CTX GIIIA (left) and A22E (right), the peptide backbone is displayed in ribbon format. Residue 22 is rendered in CPK format. The critical R13 is highlighted in stick format.

$$\Omega = (IC_{50}^{\text{mutated toxin}-\text{WT channel}}/IC_{50}^{\text{WT toxin}-\text{WT channel}})/$$

$$(IC_{50}^{\text{mutated toxin}-\text{mutated channel}}/IC_{50}^{\text{WT toxin}-\text{mutated channel}})$$

$$\Delta\Delta G = RT \ln \Omega$$

The standard errors for $\Delta\Delta G$ were estimated by dividing the square root of the sum of the variances of the $RT \ln IC_{50}$ means by the square root of the degree of freedom. Data reported are mean ± S.E.M. Statistical significance was determined using a paired Student's *t*-test at the 5% level.

3. Results and discussion

We first performed ^{1}H NMR spectroscopy to compare the 3D structures of native μ-CTX and the toxin analog A22E. Fig. 1A shows the chemical shift value of the α-proton of each of the 22 amino acids of μ-CTX and A22E compared with the value of the random coil [19]. The α-proton chemical shifts of all residues of A22E, except for the substituted glutamate at position 22, were indistinguishable from those measured for μ-CTX. These data show that the backbone 3D structure of A22E is very similar to that of μ-CTX. Therefore, we constructed the 3D model structure of A22E by replacing Ala-22 of μ-CTX with Glu (Fig. 1B). Note that the substituted glutamate at toxin position 22 does not appear to sterically interfere with other toxin residues known to be important in mediating Na^+ channel block in this model structure of A22E.

Having verified that the toxin 3D structure was not disrupted by the charge-change glutamate substitution, we studied the effect of A22E mutation on toxin affinity. When applied to WT μ1 Na^+ channels, A22E significantly reduced μ-CTX block ($P < 0.05$). The half-blocking concentrations (IC_{50}) of μ-CTX and A22E estimated from the dose–response curves shown in Fig. 2 were 30.7 ± 6.2 nM ($n = 6$) and 2.8 ± 0.3 μM ($n = 6$), respectively. These results hint at the presence of significant repulsion between the substituted glutamate and negative charges within the pore receptor. We scanned the channel interacting partner(s) of A22E by first determining the IC_{50} for block of Y401K, Y401A, E758Q, D762K, D762A, E765K, E765A and D1241K channels by μ-CTX and A22E (Fig. 3A,B). These channel sites were chosen because they line the Na^+ channel pore and are known to influence μ-CTX block [11–14,16,20,21]. Similar to that seen with WT μ1, the analog A22E blocked all pore mutants less potently than did native μ-CTX with the same channels. In fact, we were unable to block Y401K and D1241K channels even with up to 10 μM A22E. The difference in block potency between μ-CTX and A22E was smallest for E765K channels.

To quantitate the strength of the molecular coupling between E22 and the various pore sites, we employed thermodynamic mutant cycle analysis to estimate the individual interaction energies ($\Delta\Delta G$) for each of the toxin–channel pairs from their corresponding IC_{50} values (Fig. 3C). Couplings (Ω, $\Delta\Delta G$) of A22E with all channel mutants studied were < 1.0 kcal/mol (i.e. $\Omega < 5$), except for E765K whose interaction with A22E was exceptionally strong ($\Omega = 40.0$, $\Delta\Delta G = 2.2 \pm 0.1$ kcal/mol), indicating an overall gain of total coupling energy when A22E was applied to the lysine-substituted E765K channels. However, this positive coupling was not observed even with the A22E–E765A pair, indicating that a complementary pair of charges is needed to create a positive interaction between these sites. The couplings of A22E with Y401K and D1241K could not be precisely determined because of the lack of sensitivity of these channels to A22E. However, a coupling comparable to that observed for the A22E–E765K pair would predict an IC_{50} of about 20 μM for A22E block of Y401K and D1241K channels, which in turn would predict ~33% current blockade by 10 μM A22E given that μ-CTX and Na^+ channels are known to interact

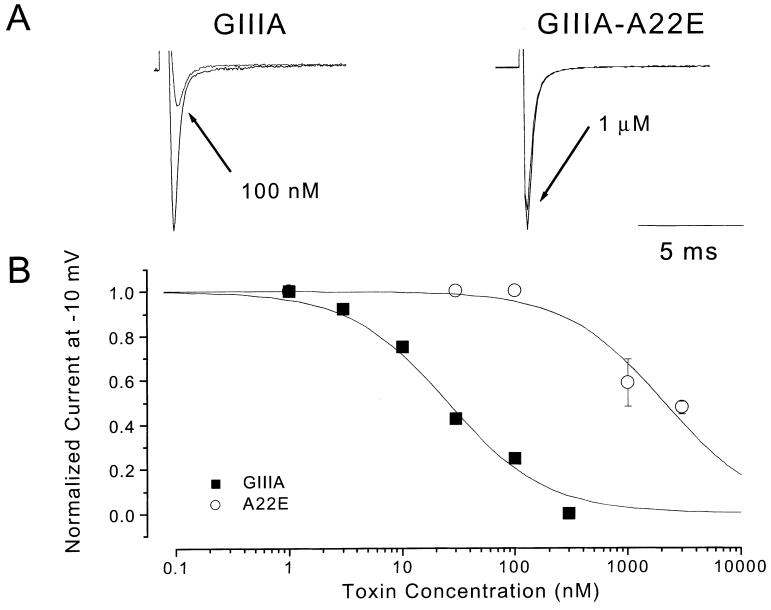

Fig. 2. Effects of the substitution A22E on μ-CTX GIIIA block of rat skeletal muscle (μ1), Na^+ channels. A: Representative raw current tracings through WT μ1 Na^+ channels recorded in the absence and presence of WT μ-CTX GIIIA (broken lines) and GIIIA-based A22E (solid lines). Currents were elicited by membrane depolarization to −10 mV from a holding potential of −100 mV. Peak currents were normalized to those recorded under toxin-free conditions. B: The dose–response relationships for μ-CTX GIIIA (solid squares) and A22E (open circles) block of μ1 Na^+ channels. Normalized peak currents were plotted as a function of extracellular toxin concentrations.

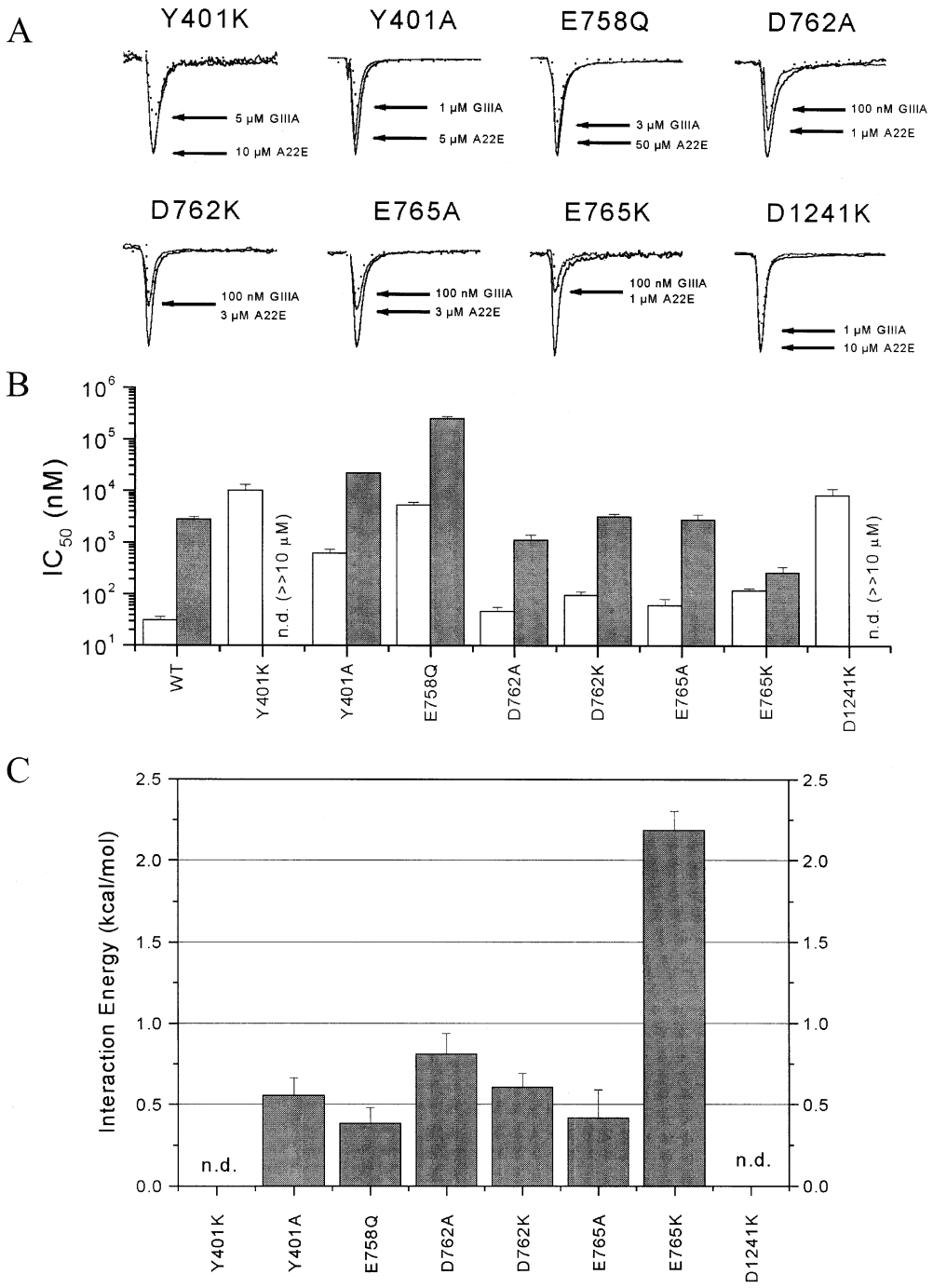

Fig. 3. Block of mutant μ1 Na^+ channels by GIIIA–A22E. A: Representative Na^+ currents through Y401K, Y401A, E758Q, D762K, D762A, E765K, E765A and D1241K channels recorded in the absence and presence of μ-CTX GIIIA (broken lines) and A22E (solid lines) as indicated. B: IC_{50} summary of the same channels as in A for block by μ-CTX GIIIA and A22E. C: Coupling energies ($\Delta\Delta G$) of A22E. A22E is strongly coupled to E765K from DII. n.d.: not determined.

with a 1:1 stoichiometry (i.e. a Hill coefficient of 1 in the binding isotherm) [11,12]. This was clearly not observed. Knowing that none of the lysine mutants (including D762K from DII) except E765K showed preferential coupling with A22E, it is reasonable to conclude that the interaction observed between these sites was site-specific. Since the binding orientation of μ-CTX is constrained by multiple toxin–channel interactions [5,11,12,22], A22E is unlikely to dock onto the pore differently from the native toxin when only a single toxin residue is substituted. Therefore, our observations suggest that residues 22 and 765 are closely associated with each other in the toxin–channel complex.

To obtain mechanistic insights into the positive interaction between A22E and E765K channels, we studied the underlying changes in blocking kinetics (Fig. 4). We measured the time courses of onset and offset of block and fitted the data with a single-exponential function (see Section 2). The resulting time constants from these fits were used to calculate the corresponding toxin association and dissociation rate constants. Notably, when compared to WT μ1, the channel mu-

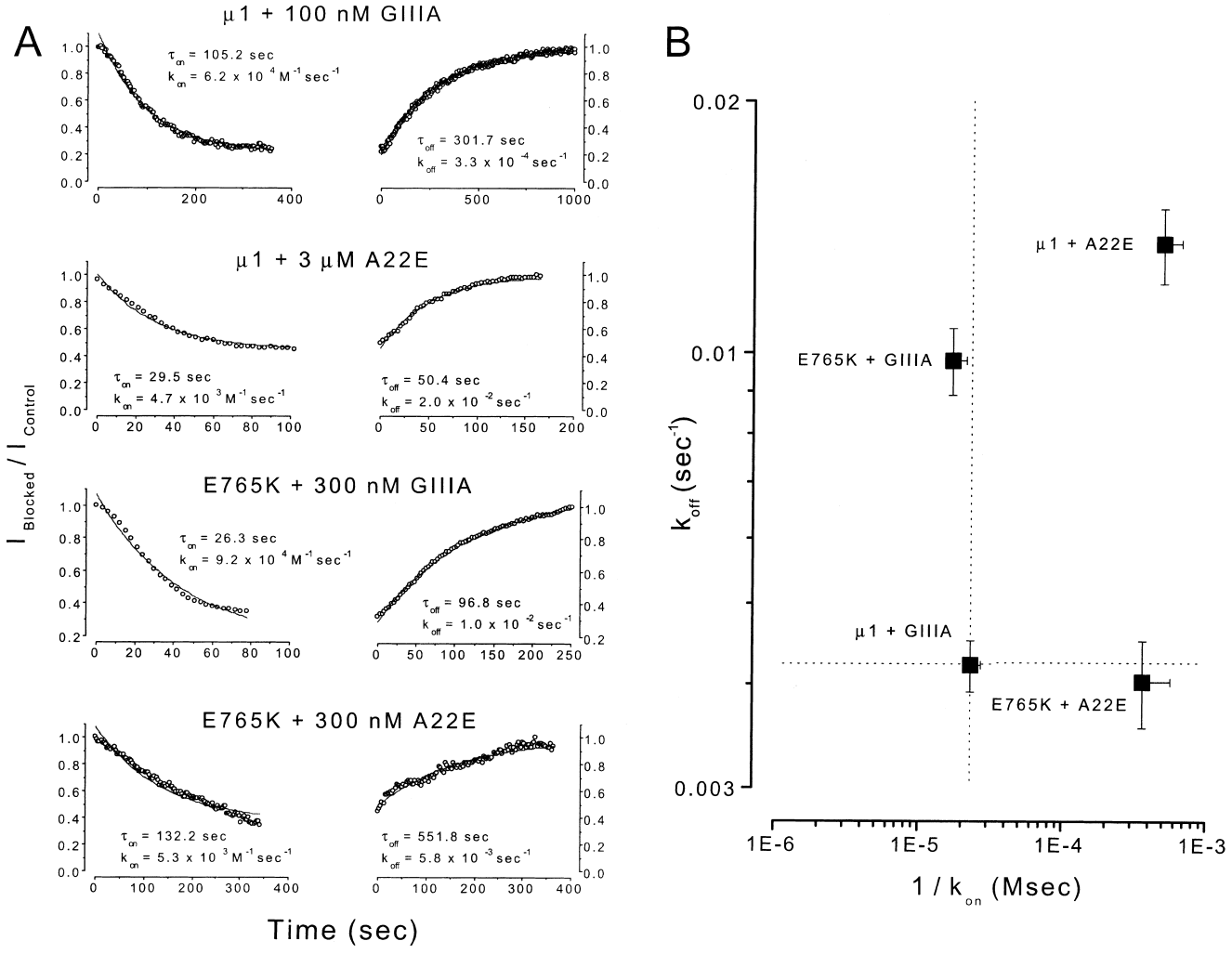

Fig. 4. Kinetic analysis of Na^+ channel block by μ-CTX and the derivative A22E. A: Time course of the development of onset and offset of μ-CTX and A22E block of WT and E765K channels during toxin washin (left panels) and washout (right panels). The corresponding time and rate constants derived from each of these experiments are indicated. B: Logarithmic plot of the dissociation rate constants (k_{off}) versus the reciprocal of the association rate constants (k_{on}). The horizontal and vertical dotted lines, respectively, represent the levels of $1/k_{on}$ and k_{off} for the WT channels. E765K accelerated k_{off} without affecting k_{on} of WT μ-CTX block. The toxin substitution A22E affected both k_{on} and k_{off}. When A22E peptide was applied to E765K, WT k_{off} (but not k_{on}) was restored suggesting that the interaction between E22 and K765 serves to stabilize the final toxin–channel complex exclusively.

tation E765K accelerated k_{off} (by 2.3-fold) without affecting k_{on} of μ-CTX GIIIA block. Further analysis reveals that the reduced affinity of A22E was due to a 21.3-fold reduction in k_{on} and a 3.2-fold increase in k_{off}. Interestingly, when A22E was applied to E765K, WT k_{off} but not k_{on} was restored suggesting the interaction between E22 and K765 exclusively serves to stabilize the final toxin–channel complex.

High-affinity μ-CTX binding requires that the toxin molecules fit snugly to the pore receptor, which depends on the physical shape of the toxin and its electrostatic interactions with the anionic pore. Previous studies of μ-CTX–Na^+ channel interactions have focused only on charged toxin residues since alterations of electrostatic interactions can often be readily detected. For this reason, the neutral μ-CTX sites have been largely ignored. However, as we gain additional knowledge on molecular constraints of μ-CTX binding to its pore receptor [11,12,16–18], more of these neutral toxin sites that are putatively in close association with the Na^+ channel pore become apparent. In this report, we took advantage of the sensitivity of the electrostatic approach to demonstrate the proximity between the neutral μ-CTX residue A22 and the DII Na^+ channel pore in the toxin-bound state. Our finding is entirely consistent with our recent μ-CTX docking model, which predicts that the helical receptor binding domain of μ-CTX consisting of R13, Q14(R), K16 and R19 interacts preferentially with the DII pore, and that K16 is most tightly coupled to DIII-D1241 [16,17]. Indeed, this pattern of toxin–channel interactions had led us to conclude that the four Na^+ channel domains are arranged in a clockwise configuration as viewed from the extracellular side [16]. This docking model is revised here to include our present findings, and schematically presented in Fig. 5. Overall, the strategy used in this study may be further exploited to probe the proximity between other neutral toxin sites and the pore. Future experiments involving cysteine replacements [23] of A22 and other μ-CTX residues will provide further insights into how μ-CTX

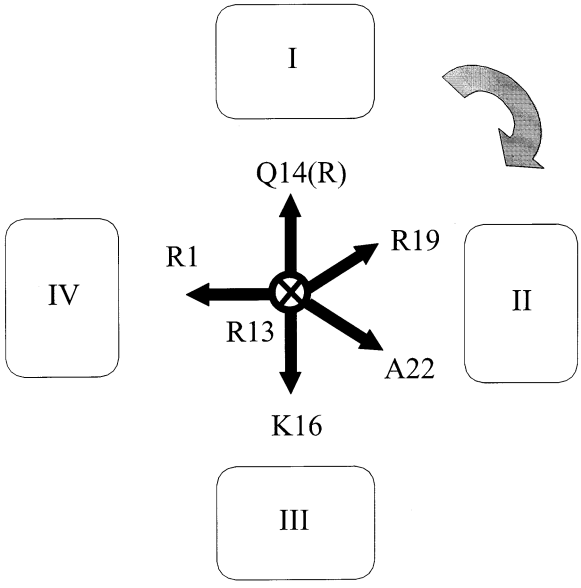

Fig. 5. Schematic diagram demonstrating the interactions of μ-CTX A22 with DII. Directional vectors indicating the relative side chain orientations of R1, Q14(R), K16, R19 and A22 are shown with respect to the R13 axis. The four Na^+ channel domains (DI–IV) are arranged in a clockwise configuration when viewed from the extracellular side [16,17]. A22 of μ-CTX associates closely with the DII pore.

sterically interacts with the contact surface of its pore receptor. Given the well-defined 3D structure of μ-CTX, a combination of these electrostatic and non-ionic approaches will help define the uncertain Na^+ channel pore contour.

Acknowledgements: This work was supported by the National Institutes of Health (R01 HL-52768 to E.M. and R01 HL-50411 to G.F.T.). R.A.L. is the recipient of a Research Career Development Award from the Cardiac Arrhythmias Research and Education Foundation. K.S. is supported in part by a Grant-in-Aid for scientific research from the Japan Society for the Promotion of Science (JSPS). E.M. holds the Michel Mirowski, M.D. Professorship of Cardiology of the Johns Hopkins University.

References

[1] Nakamura, H., Kobayashi, J., Ohizumi, Y. and Hirata, Y. (1983) Experientia 39, 590–591.
[2] Cruz, L.J., Gray, W.R., Olivera, B.M., Zeikus, R.D., Kerr, L., Yoshikami, D. and Moczydlowski, E. (1985) J. Biol. Chem. 260, 9280–9288.
[3] Hidaka, Y., Sato, K., Nakamura, H., Kobayashi, J., Ohizumi, Y. and Shimonishi, Y. (1990) FEBS Lett. 264, 29–32.
[4] Lancelin, J.M., Kohda, D., Tate, S., Yanagawa, Y., Abe, T., Satake, M. and Inagaki, F. (1991) Biochemistry 30, 6908–6916.
[5] Sato, K. et al. (1991) J. Biol. Chem. 266, 16989–16991.
[6] Wakamatsu, K. et al. (1992) Biochemistry 31, 12577–12584.
[7] Hill, J.M., Alewood, P.F. and Craik, D.J. (1996) Biochemistry 35, 8824–8835.
[8] Catterall, W.A. (1988) Science 242, 50–61.
[9] Moczydlowski, E., Olivera, B.M., Gray, W.R. and Strichartz, G.R. (1986) Proc. Natl. Acad. Sci. USA 83, 5321–5325.
[10] Yanagawa, Y., Abe, T., Satake, M., Odani, S., Suzuki, J. and Ishikawa, K. (1988) Biochemistry 27, 6256–6262.
[11] Dudley Jr., S.C., Todt, H., Lipkind, G. and Fozzard, H.A. (1995) Biophys. J. 69, 1657–1665.
[12] Li, R.A., Tsushima, R.G., Kallen, R.G. and Backx, P.H. (1997) Biophys. J. 73, 1874–1884.
[13] Li, R.A., Velez, P., Chiamvimonvat, N., Tomaselli, G.F. and Marbán, E. (1999) J. Gen. Physiol. 115, 81–92.
[14] Backx, P.H., Yue, D.T., Lawrence, J.H., Marbán, E. and Tomaselli, G.F. (1992) Science 257, 248–251.
[15] Chahine, M., Sirois, J., Marcotte, P., Chen, L. and Kallen, R.G. (1998) Biophys. J. 75, 236–246.
[16] Li, R.A., Ennis, I.I., French, R.J., Dudley Jr., S.C., Tomaselli, G.F. and Marbán, E. (2001) J. Biol. Chem. 276, 1172–1177.
[17] Li, R.A., Ennis, I.L., Tomaselli, G.F., French, R.J. and Marbán, E. (2001) Biochemistry 40, 6002–6008.
[18] Chang, N.S., French, R.J., Lipkind, G.M., Fozzard, H.A. and Dudley Jr., S. (1998) Biochemistry 37, 4407–4419.
[19] Wishart, D.S. and Sykes, B.D. (1994) Methods Enzymol. 239, 363–392.
[20] Chiamvimonvat, N., Perez-Garcia, M.T., Ranjan, R., Marbán, E. and Tomaselli, G.F. (1996) Neuron 16, 1037–1047.
[21] Li, R.A., Ennis, I.L., Velez, P., Tomaselli, G.F. and Marbán, E. (2000) J. Biol. Chem. 275, 27551–27558.
[22] Becker, S., Prusak-Sochaczewski, E., Zamponi, G., Beck-Sickinger, A.G., Gordon, R.D. and French, R.J. (1992) Biochemistry 31, 8229–8238.
[23] Nakamura, M., Niwa, Y., Ishida, Y., Kohno, T., Sato, K., Oba, Y. and Nakamura, H. (2001) FEBS Lett. 503, 107–110.